Published in final edited form as:

Int J Radiat Oncol Biol Phys. 2018 March 15; 100(4): 1016–1025. doi:10.1016/j.ijrobp.2017.12.257.

Inhibitors of HIF-1α and CXCR4 Mitigate the Development of Radiation Necrosis in Mouse Brain

Ruimeng Yang, MD[*,†], **Chong Duan, PhD**[‡], **Liya Yuan, PhD**[§], **John A. Engelbach, AS**[†], **Christina I. Tsien, MD**[‖], **Scott C. Beeman, PhD**[†], **Carlos J. Perez-Torres, PhD**[†], **Xia Ge, PhD**[†], **Keith M. Rich, MD**[§,‖], **Joseph J.H. Ackerman, PhD**[†,‡,¶,#], and **Joel R. Garbow, PhD**[†,#]

[*]Department of Radiology, Guangzhou First People's Hospital, Guangzhou Medical University, Guangzhou, China

[†]Department of Radiology, Washington University, St Louis, Missouri

[‡]Department of Chemistry, Washington University, St Louis, Missouri

[§]Department of Neurosurgery, Washington University, St Louis, Missouri

[‖]Department of Radiation Oncology, Washington University, St Louis, Missouri

[¶]Department of Medicine, Washington University, St Louis, Missouri

[#]Alvin J. Siteman Cancer Center, Washington University, St Louis, Missouri

Abstract

Purpose—There is mounting evidence that, in addition to angiogenesis, hypoxia-induced inflammation via the hypoxia-inducible factor 1α (HIF-1α)–CXC chemokine receptor 4 (CXCR4) pathway may contribute to the pathogenesis of late-onset, irradiation-induced necrosis. This study investigates the mitigative efficacy of an HIF-1α inhibitor, topotecan, and a CXCR4 antagonist, AMD3100, on the development of radiation necrosis (RN) in an intracranial mouse model.

Methods and Materials—Mice received a single-fraction, 50-Gy dose of hemispheric irradiation from the Leksell Gamma Knife Perfexion and were then treated with either topotecan, an HIF-1α inhibitor, from 1 to 12 weeks after irradiation, or AMD3100, a CXCR4 antagonist, from 4 to 12 weeks after irradiation. The onset and progression of RN were monitored longitudinally via noninvasive, in vivo magnetic resonance imaging (MRI) from 4 to 12 weeks after irradiation. Conventional hematoxylin-eosin staining and immunohistochemistry staining were performed to evaluate the treatment response.

Results—The progression of brain RN was significantly mitigated for mice treated with either topotecan or AMD3100 compared with control animals. MRI-derived lesion volumes were

Reprint requests to: Joel R. Garbow, PhD, Biomedical MR Laboratory, Campus Box 8227, Washingtobn University School of Medicine, Room 2313, 4525 Scott Ave, St Louis, MO 63110. Tel: (314) 362-9949; garbow@wustl.edu.

R.Y. and C.D. contributed equally to this work.

J.R.G. was responsible for the statistical analysis.

Conflict of interest: none.

Supplementary material for this article can be found at www.redjournal.org.

significantly smaller for both of the treated groups, and histologic findings correlated well with the MRI data. By hematoxylin-eosin staining, both treated groups demonstrated reduced irradiation-induced tissue damage compared with controls. Furthermore, immunohistochemistry results revealed that expression levels of vascular endothelial growth factor, CXC chemokine ligand 12, CD68, CD3, and tumor necrosis factor α in the lesion area were significantly lower in treated (topotecan or AMD3100) brains versus control brains, while ionized calcium-binding adapter molecule 1 (Iba1) and HIF-1α expression was similar, though somewhat reduced. CXCR4 expression was reduced only in topotecan-treated mice, while interleukin 6 expression was unaffected by either topotecan or AMD3100.

Conclusions—By reducing inflammation, both topotecan and AMD3100 can, independently, mitigate the development of RN in the mouse brain. When combined with first-line, antiangiogenic treatment, anti-inflammation therapy may provide an adjuvant therapeutic strategy for clinical, postirradiation management of tumors, with additional benefits in the mitigation of RN development.

Introduction

Late time–to–onset brain radiation necrosis (RN), a well-known adverse effect following radiation therapy for central nervous system (CNS) tumors, is a serious clinical problem (1, 2). With combined chemoradiation therapy as the current standard of care for the majority of CNS tumors, the incidence of RN has substantially increased (3). Treatment-induced effects can appear from as few as 3 months to as many as ≥ 10 years after radiation therapy (1). Both medical and surgical management strategies have been used to treat RN. Current medical treatments, including corticosteroids (4), hyperbaric oxygen therapy (5), and anticoagulants or antiplatelet agents (6), either are associated with significant toxicity or have limited efficacy. Surgical resection is typically reserved for symptomatic patients because of mass effect and is associated with potential morbidity and death (7).

To overcome this clinically challenging pathology, numerous studies have focused on unraveling the mechanisms underlying the development and/or progression of RN and discovering new molecular targets that might facilitate novel treatments (1, 2, 8–10). In those studies, in addition to angiogenesis, inflammation via the hypoxia-inducible factor 1α (HIF-1α)–CXC chemokine receptor 4 (CXCR4) pathway has been hypothesized as an important contributor to the pathogenesis of brain RN. In brief, focal endothelial damage and associated local tissue hypoxia following irradiation induce HIF-1α expression, which strongly mediates upregulation of vascular endothelial growth factor (VEGF). VEGF plays an important role in both increased angiogenesis and vascular permeability. Meanwhile, radiation therapy–associated increases in the cytokine signaling cascade lead to increased inflammation, with astrocytes that express CXC chemokine ligand 12 (CXCL12, also known as stromal derived factor 1) recruiting monocytes (ie, microglia and macrophages) and lymphocytes expressing CXCR4 via CXCL12-CXCR4 chemotaxis. Furthermore, these monocytes and lymphocytes contribute to further inflammation by releasing inflammatory cytokines, including tumor necrosis factor α (TNF-α), interleukin 6 (IL-6), and NF-κB (nuclear factor kappa-light-chain-enhancer of activated B cells). Increased angiogenesis and

inflammation exacerbate tissue hypoxia and vasogenic edema, resulting in continued progression of CNS RN.

Bevacizumab (Avastin; Genentech, San Francisco, CA), a monoclonal anti-VEGF antibody that prevents VEGF from reaching its endothelial targets (11, 12), thereby reducing the associated treatment-related edema, has been recognized as an effective therapy for treating RN and reducing perilesional edema clinically (13, 14). Furthermore, our preclinical studies have validated the mitigative effect of the analogous murine anti-VEGF antibody (B20-4.1.1) on RN (15) in a murine model of late-onset RN (16). However, many clinical studies have reported that the efficacy of bevacizumab in treating RN is transitory, and RN may recur or progress after bevacizumab treatment is discontinued (17–19). Treatment side effects, including deep vein thrombosis and focal mineralization, have also been documented (13, 20).

It has been widely known that overexpression of HIF-1α correlates significantly with tumor invasion and metastasis (21–23). Hypoxia-induced CXCR4 expression has also been implicated in many tumors (24, 25). Blocking the HIF-1α–CXCR4 signaling pathway, using an HIF-1α inhibitor or CXCR4 antagonist, can inhibit tumor growth and retard potential metastasis (23, 26). However, whether the HIF-1α–CXCR4 pathway plays a critical role in the progression of RN has not been elucidated conclusively. We have recently developed and characterized a mouse model of late-onset RN that recapitulates all of the histologic features of RN observed in patients (15). In the present study, the mitigative efficacy of inhibiting the HIF-1α–CXCR4 signaling pathway of RN was evaluated by longitudinal, in vivo magnetic resonance imaging (MRI) and immunohistochemistry (IHC).

Methods and Materials

Animals

All experimental procedures involving animals were approved by Washington University Institutional Animal Care and Use Committee and conformed with the National Institutes of Health policy on responsibility for care and use of animals. We used 7- to 8-week-old female BALB/c mice (Envigo, Indianapolis, IN) in the study.

Irradiation

Mice were irradiated with a single fraction of 50 Gy (50% isodose) of irradiation, as previously described (15). Unlike clinical radiation therapy, which seeks to avoid damage to normal brain tissue, this dose was chosen specifically to produce late time–to–onset RN in mice in an experimentally tractable time frame (ie, 4–5 weeks after irradiation). In brief, mice were anesthetized and restrained on a custom-made platform mounted to the stereotactic frame that attaches to the treatment couch of the Leksell Gamma Knife (GK) Perfexion treatment unit (Elekta, Stockholm, Sweden), a state-of-the-art device used for stereotactic irradiation of patients with malignant brain tumors. Mice were anesthetized with a mixture of ketamine (25 mg/kg), acepromazine (5 mg/kg), and xylazine (5 mg/kg) and underwent an intraperitoneal injection 5 minutes before the start of irradiation. A single radiation fraction of 50 Gy (50% isodose) was focused on the cortex of the left hemisphere,

approximately 3 mm posterior to the bregma. At this dose, the onset of RN typically occurs at approximately 4 weeks after irradiation (27). While comparisons are inexact, we note that laboratory mice have roughly half the radiation sensitivity (ie, lethal dose, 50%, LD_{50}) of humans (28, 29). Thus, the 50-Gy mouse irradiation dose corresponds approximately to a 25-Gy human exposure.

HIF-1α and CXCR4 inhibitors

Topotecan (Cayman Chemicals, Ann Arbor, MI), a topoisomerase I inhibitor, nonselectively suppresses HIF-1α expression (30) and causes concomitant inhibition of HIF-1α target genes, angiogenesis, and tumor growth (31). AMD3100 (Cayman Chemicals), a symmetrical bicyclam ie, an antagonist of CXCR4, has been widely used to block the CXCL12-CXCR4 chemotaxis (32, 33). Both topotecan and AMD3100 have received US Food and Drug Administration approval and have been used clinically in the treatment of brain tumors and other tumors (31, 34).

Experimental scheme

Two treatment groups, designated groups A and B, were included in this study. Group A mice were used to investigate the efficacy of HIF-1α inhibition via topotecan as a treatment of RN. Following GK irradiation, mice were randomly divided into 2 cohorts. Mouse cohort A1 (n=8) received topotecan (10 mg/kg in dimethyl sulfoxide [DMSO]), while mouse cohort A2 (n=7) received an equivalent volume of DMSO, intraperitoneally twice weekly from 1 to 12 weeks after irradiation.

Group B mice were used to determine the efficacy of CXCR4 inhibition via AMD3100 on the treatment of RN. At week 4 after irradiation, mice were randomly divided into 2 cohorts. Mouse cohort B1 (n=7) received AMD3100 (5 mg/kg), while mouse cohort B2 (n=6) received the equivalent volume of phosphate-buffered saline solution (PBS, pH 7.4), intraperitoneally daily from 4 to 12 weeks after irradiation.

Doses of topotecan and AMD3100 were chosen based on previously published studies on mouse brain tumors (31, 35, 36). In experiment A, the anti–HIF-1α treatment started from week 1 after irradiation, as it has been shown that local hypoxia, which mediates the upregulation ofHIF-1α, was induced soon after irradiation (2). In experiment B, the treatment with AMD3100 started from week 4 after irradiation, which was the earliest time at which focal RN lesions could be observed on anatomic magnetic resonance (MR) images (16).

Magnetic resonance imaging

In vivo MRI experiments were performed on a 4.7-T small-animal MR scanner (Agilent Technologies [Varian], Santa Clara, CA) equipped with a DirectDrive console (Agilent Technologies). MRI data were collected using an actively decoupled coil pair. Before being placed into the magnet, mice underwent an intraperitoneal injection of 0.25 mL of MultiHance contrast agent (gadobenate dimeglumine; Bracco Diagnostics, Princeton, NJ), diluted 2:10 in sterile saline solution (more detailed information is provided in Appendix E1; available online at www.redjournal.org).

All mice in experiment A were imaged every two weeks from 4 to 12 weeks after irradiation. In experiment B, mouse cohort B1 was imaged weekly from 4 to 12 weeks after irradiation while cohort B2 mice were imaged every two weeks from 4 to 12 weeks after irradiation. It should be noted that contrast agent clears completely between imaging sessions. For both experiments, multislice, spin-echo, T2-weighted images were collected with the following parameters: time to repetition, 1200 ms; time to echo, 50 ms; number of transients, 4; field of view, 15 × 15 mm^2; matrix size, 128 × 128; slice thickness, 0.5 mm; and 21 slices to cover the whole brain. Multislice, spin-echo, postcontrast, T1-weighted images were acquired with the same field of view and slice coverage, with the following parameters: time to repetition, 650 ms; time to echo, 20 ms; and number of transients, 4.

Data analysis and statistics

All datasets were analyzed, as previously described (15, 37), using custom-written MATLAB software (The MathWorks, Natick, MA). In brief, each mouse brain was divided along the midline into left (irradiated) and right (nonirradiated) hemispheres. The lesion was defined as the region of hyperintensity on postcontrast T1-or T2-weighted MR images. MR-derived lesion volumes were determined via a threshold segmentation algorithm, in which areas of the left hemisphere brighter than the 95th percentile of the right hemisphere were defined as lesions. (The lesion volume is then the sum of the lesion voxels multiplied by the voxel volume.) Repeated-measures 2-way analysis of variance with Bonferroni post-tests was used to compare the tumor volumes across groups at selected time points after irradiation. Graphs and statistical analyses were performed using Prism (GraphPad Software, San Diego, CA) and MATLAB software.

Histology and IHC

Tissue sections were stained with hematoxylin-eosin (H&E), per standard protocols. In addition, IHC staining for HIF-1α, VEGF, CXCR4, CXCL12, Iba1, CD68, CD3, TNF-α, and IL-6 was performed following the manufacturer's procedures. In brief, mice were killed humanely and underwent intracardiac perfusion with 1% PBS, followed by 10% formalin, immediately after the final imaging session. Each mouse head was dissected and immersed in 10% formalin for 24 hours. The brains were extracted from the skulls, and a 2-mm-thick coronal block, centered at the irradiation site (approximately 3 mm posterior to the bregma), was obtained for each brain. The blocks were embedded in paraffin wax and sectioned from the center, at a thickness of 5 μm. All sections were deparaffinized and rehydrated; antigen retrieval was performed with citrate buffer (pH 6.8) at 70°C overnight, following 1-hour nonspecific blocking using an avidin-biotin complex blocking kit (Life Technologies, Grand Island, NY). All primary antibodies were incubated with sections at 4°C overnight (more detailed information is provided in Appendix E1; available online at www.redjournal.org). All sections were processed with the Histostain Plus Broad System kit (Invitrogen Life Technologies, Frederick, MD) followed by a broad-spectrum secondary antibody for 1 hour. Three percent hydrogen peroxide was used to decrease the background. Histologic sections were examined with the Hamamatsu Nano-Zoomer whole-slide imaging system (Hamamatsu, Hamamatsu, Japan). For each animal, each IHC stain was graded on a scale from 0 to 3 (ie, 0, no stain; 1, light stain; 2, moderate stain; and 3, heavy stain) by an experienced histologist (L.Y.).

Results

Both HIF-1α inhibitor, topotecan, and CXCR4 antagonist, AMD3100, slow progression of RN in mouse brain

Figure 1A and 2A show representative postcontrast, T1-and T2-weighted MR images at weeks 4, 8, and 12 after irradiation for each mouse cohort. Heterogeneous, hyperintense areas in these images correspond to RN lesions in the brain. The DMSO-treated and PBS-treated brains showed larger lesions at week 8 after irradiation, and the lesions progressed significantly by week 12 after irradiation. By contrast, topotecan-treated and AMD3100-treated brains showed minimal hyperintense areas until week 8 after irradiation. Figure 1B and 2B are plots of RN lesion volume versus weeks after irradiation derived from T1-and T2-weighted MR images. For the mice treated with top-otecan, these plots showed significantly smaller RN lesion volumes at weeks 8, 10, and 12 after irradiation compared with mice treated with carrier only. In a similar manner, AMD3100 treatment significantly decreased RN volume, beginning 6 weeks after irradiation, compared with the PBS-treated mice.

H&E staining proves that both topotecan and AMD3100 mitigate RN in irradiated brain tissue

Figure 3 shows representative H&E histologic images for treated and control mice from both experiments A and B at 12 weeks after irradiation. The irradiated hemispheres of the DMSO-treated mice (Fig. 3A, left column) and PBS-treated mice (Fig. 3B, left column) demonstrated histologic hallmarks of RN, including fibrinoid vascular necrosis (yellow arrow), vascular telangiectasia (black arrow), hemorrhage (blue arrows), loss of neurons, and edema (green arrows). By contrast, the irradiated hemisphere of the topotecan-treated mice (Fig. 3A, middle and right columns) and AMD3100-treated mice (Fig. 3B, middle and right columns) showed only mild to modest tissue damage. These histologic findings support the MR data shown in Figure 1A and 2A, demonstrating the mitigative effect of HIF-1α and CXCR4 inhibition on RN development and progression. The mixed pathologic features seen in the H&E-stained sections also explain the heterogeneous signals observed on postcontrast T1-and T2-weighted images.

IHC staining demonstrates that both topotecan and AMD3100 reduce inflammation in irradiated mice

Figure 4 shows representative IHC staining for molecular markers of microglia and immune cells (macrophages and lymphocytes) in mouse brains from experiments A (Fig. 4A) and B (Fig. 4B). The number of Iba1-labeled microglia was similar, although somewhat lower, in the brains of topotecan-or AMD3100-treated mice compared with those of the carrier-treated animals. In addition, there were no clusters of positively Iba1-stained cells in either topotecan- or AMD3100-treated RN brain slices, while such clusters could be seen clearly in the brains of control mice (data not shown). CD68-labeled macrophages and CD3-labeled lymphocytes were observed, predominantly on the edges of RN lesions and surrounding the damaged vascular vessels. Both top-otecan and AMD3100 dramatically reduced the numbers of CD68-and CD3-positive cells in treated mice.

Figure 5 shows representative IHC staining for the expression of HIF-1α, VEGF, CXCR4, CXCL12, TNF-α, and IL-6 in mouse brains from both experiments A (Fig. 5A) and B (Fig. 5B). The results of scoring the IHC-stained slides, as described in the "Methods and Materials" section, are reported in Table 1. Values in Table 1 represent the average score across all animals within each treatment or control group. Compared with the control group, treatment with either topotecan or AMD3100 resulted in reduced expression of VEGF in the radiated mouse brain while HIF-1α expression was largely unchanged. Expression of CXCL12 was clearly reduced in the brains of either topotecan- or AMD3100-treated animals relative to their control counterparts, while CXCR4 expression was reduced only in topotecan-treated mice. Treatment with either top-otecan or AMD3100 reduced the expression of the proinflammatory cytokine TNF-α but had no measurable effect on IL-6 expression.

Discussion

In a recent retrospective review of IHC analyses of surgical human RN specimens designed to elucidate the molecular mechanisms underlying brain RN, Yoritsune et al (2) found that both angiogenesis and inflammation may be caused by the upregulation of HIF-1α after radiation therapy. HIF-1α not only contains a transactivation domain for VEGF but also is an important regulator of the CXCL12-CXCR4 chemokine axis (2, 38, 39), whose activity is thought to be significantly upregulated under both hypoxia and inflammation (40, 41). Accumulated proinflammatory cytokines in the perinecrotic area would, in turn, aggravate hypoxia and, consequently, further upregulate HIF-1α (ie, positive feedback). CXCR4 activation by CXCL12 plays a key role within hypoxic areas of tumors by enabling increased cell growth, invasiveness, and recruitment of endothelial cell progenitors, leading to tumor angiogenesis. A CXCR4 antagonist demonstrated inhibition of intracranial glioblastoma xenograft tumor cell growth by increased apoptosis through acting on the CXCL12-CXCR4 axis (34, 42). VEGF and CXCR4 antagonists are potential therapeutic agents that may be used to both mitigate RN and inhibit glioma tumor cell growth. Thus, in this study we sought to investigate the role of hypoxia and inflammation on the progression and/or development of GK-induced late time–to–onset RN via the use of an HIF-1α inhibitor, topotecan, and a CXCR4 antagonist, AMD3100.

The onset and progression of RN in the mouse brain were characterized by heterogeneous, hyperintense regions detected on either postcontrast T1-or T2-weighted images (Fig. 1A and 2A). Differences between T1-and T2-weighted image–defined lesion boundaries—thus volumes—reflect the different contrast mechanisms of these MRI protocols, blood-brain barrier breakdown and edema, respectively. Compared with controls, irradiated brains of mice treated with either topotecan or AMD3100 demonstrated significantly smaller lesion volumes, as measured longitudinally by in vivo MRI; reduced swelling; and decreased RN-related tissue damage, assessed in H&E-stained tissue sections. These results demonstrate clearly the efficacy of both topotecan and AMD3100 in mitigating the progression of RN in mice.

To validate that treatments with topotecan or AMD3100 reduce inflammation via the hypoxia–HIF-1α–CXCR4 pathway, IHC staining of brain slices for HIF-1α, VEGF,

CXCR4, CXCL12, Iba1, CD68, and CD3 was performed. Initially, we focused on detecting changes in microglia, macrophages, and lymphocytes, cells that are widely recognized to be involved in the progression of inflammation in the CNS. The decreased expression of CD68 and CD3, as well as the somewhat lower expression of Iba1, measured via IHC staining at 12 weeks after irradiation suggests that both topotecan and AMD3100 treatments attenuate microglia activation and macrophage and lymphocyte infiltration.

Topotecan is a negative regulator of the CXCL12-CXCR4 chemokine axis, while AMD3100 is an antagonist of CXCR4. Treatment with either topotecan or AMD3100 in our study markedly impaired CXCL12 expression, while topotecan reduced expression of CXCR4, thereby providing strong evidence that both topotecan and AMD3100 can deactivate the CXCL12-CXCR4 signaling pathway. (As an antagonist of CXCR4, AMD3100 blocks the action of CXCR4, without reducing its expression.) However, HIF-1α expression was largely unaffected by either treatment, suggesting that both topotecan and AMD3100 act predominantly on downstream expression of VEGF and CXCL12, an effect that might be due to the reduced positive feedback effect of proinflammatory cytokines. To test this notion, the expressions of proinflammatory cytokines, including TNF-α and IL-6, were evaluated. Consistent with the staining results for immune cells (ie, macrophages and lymphocytes), which are able to produce these cytokines, both topotecan treatment and AMD3100 treatment resulted in reduced TNF-α expression. However, there was no obvious decrease in IL-6 expression after treatment. This finding suggests that signaling pathways such as NF-κB–associated increases in IL-6 activation with associated Janus kinases (JAKs), as well as signal transducer and activator of transcription (STAT) 3 transcription factor, may play a role in the progression of RN. However, further study is needed to investigate and validate these observations.

Conclusions

Irradiation is a powerful and ubiquitous treatment for brain tumors. However, its outcome may be complicated by the appearance of delayed RN. Blocking the HIF-1α–CXCR4 pathway axis with topotecan or AMD3100 results in significant antitumor activity against many types of cancer in vitro and in vivo and, importantly, inhibits the development of metastases and cancer tumor cell growth and invasion (31, 43–50). The results of this study demonstrate that treatment with topotecan or AMD3100 can also significantly inhibit the HIF-1α–CXCR4 axis, thereby reducing the progression of RN. Targeting the HIF-1α–CXCR4 pathway may be a promising therapy for treating recurrent tumor after radiation therapy, with the additional benefit of mitigating the progression of RN.

Supplementary Material

Refer to Web version on PubMed Central for supplementary material.

Acknowledgments

This project was supported by National Institutes of Health grant R01 CA155365 (J.R.G.), the Alvin J. Siteman Cancer Center Siteman Investment Program (supported by The Foundation for Barnes-Jewish Hospital, Cancer Frontier Fund; National Cancer Institute, Cancer Center Support Grant, P30 CA091842; and, Barnard Trust), Elekta

Instruments AB (Stockholm, Sweden), Guangdong Natural Science Foundation (2014A030313647), and the Science and Technology Plan Foundation of Guangzhou (201607010038).

The authors thank Dr Robert Drzymala and Mr Jeremy Cates (Radiation Oncology, Washington University) for their assistance in generating the radiation necrosis mouse model.

References

1. Furuse M, Nonoguchi N, Kawabata S, et al. Delayed brain radiation necrosis: Pathological review and new molecular targets for treatment. Med Mol Morphol. 2015; 48:183–190. [PubMed: 26462915]
2. Yoritsune E, Furuse M, Kuwabara H, et al. Inflammation as well as angiogenesis may participate in the pathophysiology of brain radiation necrosis. J Radiat Res. 2014; 55:803–811. [PubMed: 24676944]
3. Kumar AJ, Leeds NE, Fuller GN, et al. Malignant gliomas: MR imaging spectrum of radiation therapy- and chemotherapy-induced necrosis of the brain after treatment. Radiology. 2000; 217:377–384. [PubMed: 11058631]
4. Shaw PJ, Bates D. Conservative treatment of delayed cerebral radiation necrosis. J Neurol Neurosurg Psychiatry. 1984; 47:1338–1341. [PubMed: 6512555]
5. Bui QC, Lieber M, Withers HR, et al. The efficacy of hyperbaric oxygen therapy in the treatment of radiation-induced late side effects. Int J Radiat Oncol Biol Phys. 2004; 60:871–878. [PubMed: 15465205]
6. Glantz MJ, Burger PC, Friedman AH, et al. Treatment of radiation-induced nervous system injury with heparin and warfarin. Neurology. 1994; 44:2020–2027. [PubMed: 7969953]
7. McPherson CM, Warnick RE. Results of contemporary surgical management of radiation necrosis using frameless stereotaxis and intraoperative magnetic resonance imaging. J Neurooncol. 2004; 68:41–47. [PubMed: 15174520]
8. Yoshii Y. Pathological review of late cerebral radionecrosis. Brain Tumor Pathol. 2008; 25:51–58. [PubMed: 18987829]
9. Nonoguchi N, Miyatake S, Fukumoto M, et al. The distribution of vascular endothelial growth factor-producing cells in clinical radiation necrosis of the brain: Pathological consideration of their potential roles. J Neurooncol. 2011; 105:423–431. [PubMed: 21688077]
10. Miyatake S, Nonoguchi N, Furuse M, et al. Pathophysiology, diagnosis, and treatment of radiation necrosis in the brain. Neurol Med Chir (Tokyo). 2015; 55:50–59.
11. Kreisl TN, Kim L, Moore K, et al. Phase II trial of single-agent bevacizumab followed by bevacizumab plus irinotecan at tumor progression in recurrent glioblastoma. J Clin Oncol. 2009; 27:740–745. [PubMed: 19114704]
12. Matuschek C, Bolke E, Nawatny J, et al. Bevacizumab as a treatment option for radiation-induced cerebral necrosis. Strahlenther Onkol. 2011; 187:135–139. [PubMed: 21336713]
13. Levin VA, Bidaut L, Hou P, et al. Randomized double-blind placebo-controlled trial of bevacizumab therapy for radiation necrosis of the central nervous system. Int J Radiat Oncol Biol Phys. 2011; 79:1487–1495. [PubMed: 20399573]
14. Tye K, Engelhard HH, Slavin KV, et al. An analysis of radiation necrosis of the central nervous system treated with bevacizumab. J Neurooncol. 2014; 117:321–327. [PubMed: 24504500]
15. Jiang X, Engelbach JA, Yuan L, et al. Anti-vegf antibodies mitigate the development of radiation necrosis in mouse brain. Clin Cancer Res. 2014; 20:2695–2702. [PubMed: 24647570]
16. Perez-Torres CJ, Yuan L, Schmidt RE, et al. Specificity of vascular endothelial growth factor treatment for radiation necrosis. Radiother Oncol. 2015; 117:382–385. [PubMed: 26376163]
17. Furuse M, Kawabata S, Kuroiwa T, et al. Repeated treatments with bevacizumab for recurrent radiation necrosis in patients with malignant brain tumors: A report of 2 cases. J Neurooncol. 2011; 102:471–475. [PubMed: 20694573]
18. Zhuang H, Yuan X, Sun D, et al. Acquired-resistance of bevacizumab treatment for radiation brain necrosis: A case report. Oncotarget. 2016; 7:13265–13268. [PubMed: 26933810]

19. Jeyaretna DS, Curry WT Jr, Batchelor TT, et al. Exacerbation of cerebral radiation necrosis by bevacizumab. J Clin Oncol. 2011; 29:e159–e162. [PubMed: 21149667]
20. Duan C, Perez-Torres CJ, Yuan L, et al. Can anti-vascular endothelial growth factor antibody reverse radiation necrosis? A preclinical investigation. J Neurooncol. 2017; 133:9–16. [PubMed: 28425047]
21. Guo M, Cai C, Zhao G, et al. Hypoxia promotes migration and induces CXCR4 expression via HIF-1alpha activation in human osteosarcoma. PLoS One. 2014; 9:e90518. [PubMed: 24618817]
22. Semenza GL. The hypoxic tumor microenvironment: A driving force for breast cancer progression. Biochim Biophys Acta. 2016; 1863:382–391. [PubMed: 26079100]
23. Guan G, Zhang Y, Lu Y, et al. The HIF-1alpha/CXCR4 pathway supports hypoxia-induced metastasis of human osteosarcoma cells. Cancer Lett. 2015; 357:254–264. [PubMed: 25444927]
24. Ishikawa T, Nakashiro K, Klosek SK, et al. Hypoxia enhances CXCR4 expression by activating HIF-1 in oral squamous cell carcinoma. Oncol Rep. 2009; 21:707–712. [PubMed: 19212630]
25. Liu YL, Yu JM, Song XR, et al. Regulation of the chemokine receptor CXCR4 and metastasis by hypoxia-inducible factor in non small cell lung cancer cell lines. Cancer Biol Ther. 2006; 5:1320–1326. [PubMed: 16929169]
26. Cronin PA, Wang JH, Redmond HP. Hypoxia increases the metastatic ability of breast cancer cells via upregulation of CXCR4. BMC Cancer. 2010; 10:225. [PubMed: 20492653]
27. Jiang X, Yuan L, Engelbach JA, et al. A gamma-knife-enabled mouse model of cerebral single-hemisphere delayed radiation necrosis. PloS One. 2015; 10:e0139596. [PubMed: 26440791]
28. French NR. Radiation sensitivity of rodent species. Nature. 1969; 222:1003–1004. [PubMed: 5789321]
29. Mole RH. The LD50 for uniform low LET irradiation of man. Br J Radiol. 1984; 57:355–369. [PubMed: 6372928]
30. Rapisarda A, Uranchimeg B, Scudiero DA, et al. Identification of small molecule inhibitors of hypoxia-inducible factor 1 transcriptional activation pathway. Cancer Res. 2002; 62:4316–4324. [PubMed: 12154035]
31. Rapisarda A, Zalek J, Hollingshead M, et al. Schedule-dependent inhibition of hypoxia-inducible factor-1alpha protein accumulation, angiogenesis, and tumor growth by topotecan in U251-HRE glioblastoma xenografts. Cancer Res. 2004; 64:6845–6848. [PubMed: 15466170]
32. Huang J, Li Y, Tang Y, et al. CXCR4 antagonist AMD3100 protects blood-brain barrier integrity and reduces inflammatory response after focal ischemia in mice. Stroke. 2013; 44:190–197. [PubMed: 23168453]
33. Prud'homme GJ. Cancer stem cells and novel targets for antitumor strategies. Curr Pharm Des. 2012; 18:2838–2849. [PubMed: 22390767]
34. Barone A, Sengupta R, Warrington NM, et al. Combined VEGF and CXCR4 antagonism targets the GBM stem cell population and synergistically improves survival in an intracranial mouse model of glioblastoma. Oncotarget. 2014; 5:9811–9822. [PubMed: 25238146]
35. Kajiyama H, Shibata K, Terauchi M, et al. Involvement of SDF-1alpha/CXCR4 axis in the enhanced peritoneal metastasis of epithelial ovarian carcinoma. Int J Cancer. 2008; 122:91–99. [PubMed: 17893878]
36. Lau BW, Kane AB. SDF1/CXCL12 is involved in recruitment of stem-like progenitor cells to orthotopic murine malignant mesothelioma spheroids. Anticancer Res. 2010; 30:2153–2160. [PubMed: 20651364]
37. Jiang X, Perez-Torres CJ, Thotala D, et al. A gsk-3beta inhibitor protects against radiation necrosis in mouse brain. Int J Radiat Oncol Biol Phys. 2014; 89:714–721. [PubMed: 24969790]
38. Kryczek I, Wei S, Keller E, et al. Stroma-derived factor (SDF-1/CXCL12) and human tumor pathogenesis. Am J Physiol Cell Physiol. 2007; 292:C987–C995. [PubMed: 16943240]
39. Liang Z, Brooks J, Willard M, et al. CXCR4/CXCL12 axis promotes VEGF-mediated tumor angiogenesis through Akt signaling pathway. Biochem Biophys Res Commun. 2007; 359:716–722. [PubMed: 17559806]
40. Dehne N, Brune B. HIF-1 in the inflammatory microenvironment. Exp Cell Res. 2009; 315:1791–1797. [PubMed: 19332053]

41. Jung YJ, Isaacs JS, Lee SM, et al. IL-1beta-mediated up-regulation of HIF-1alpha via an NFkappaB/COX-2 pathway identifies HIF-1 as a critical link between inflammation and oncogenesis. FASEB J. 2003; 17:2115–2117. [PubMed: 12958148]
42. Rubin JB, Kung AL, Klein RS, et al. A small-molecule antagonist of CXCR4 inhibits intracranial growth of primary brain tumors. Proc Natl Acad Sci U S A. 2003; 100:13513–13518. [PubMed: 14595012]
43. Rao S, Sengupta R, Choe EJ, et al. CXCL12 mediates trophic interactions between endothelial and tumor cells in glioblastoma. PLoS One. 2012; 7:e33005. [PubMed: 22427929]
44. Balkwill F. The significance of cancer cell expression of the chemokine receptor CXCR4. Semin Cancer Biol. 2004; 14:171–179. [PubMed: 15246052]
45. Yang L, Jackson E, Woerner BM, et al. Blocking CXCR4-mediated cyclic AMP suppression inhibits brain tumor growth in vivo. Cancer Res. 2007; 67:651–658. [PubMed: 17234775]
46. Liekens S, Schols D, Hatse S. CXCL12-CXCR4 axis in angiogenesis, metastasis and stem cell mobilization. Curr Pharm Des. 2010; 16:3903–3920. [PubMed: 21158728]
47. Burger JA, Stewart DJ, Wald O, et al. Potential of CXCR4 antagonists for the treatment of metastatic lung cancer. Expert Rev Anti-cancer Ther. 2011; 11:621–630.
48. Taschner-Mandl S, Schwarz M, Blaha J, et al. Metronomic topotecan impedes tumor growth of MYCN-amplified neuroblastoma cells in vitro and in vivo by therapy induced senescence. Oncotarget. 2016; 7:3571–3586. [PubMed: 26657295]
49. Ge XH, Lin Q, Ren XC, et al. Phase II clinical trial of whole-brain irradiation plus three-dimensional conformal boost with concurrent topotecan for brain metastases from lung cancer. Radiat Oncol. 2013; 8:238. [PubMed: 24125485]
50. Burris HA III, Hanauske AR, Johnson RK, et al. Activity of topotecan, a new topoisomerase I inhibitor, against human tumor colony-forming units in vitro. J Natl Cancer Inst. 1992; 84:1816–1820. [PubMed: 1331485]

Summary

The efficacy of a hypoxia-inducible factor 1α inhibitor, topotecan, and a CXC chemokine receptor 4 antagonist, AMD3100, on the development of radiation necrosis (RN) was investigated in an intracranial mouse model. Mice were irradiated with the Leksell Gamma Knife Perfexion, and the development and progression of RN were monitored longitudinally in vivo using magnetic resonance imaging, supported with correlative histology. Both topotecan and AMD3100 can, independently, mitigate the development of RN in the mouse brain by reducing inflammation.

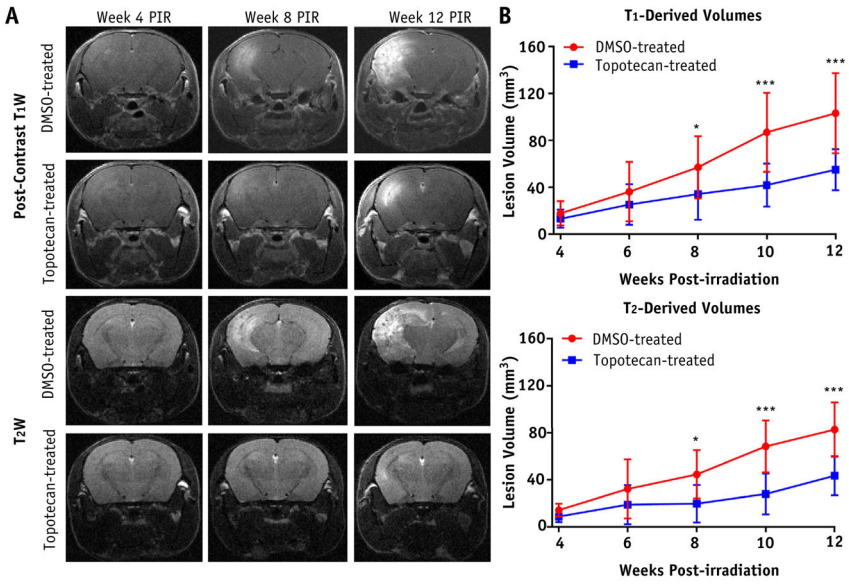

Fig. 1.

Treatment response with hypoxia-inducible factor 1α inhibitor, topotecan, as detected by anatomic magnetic resonance imaging. A, Representative postcontrast T1-weighted (T1W) images (first and second rows) and T2-weighted (T2W) images (third and fourth rows) acquired for dimethyl sulfoxide (DMSO)–treated (control) and topotecan-treated groups at 4 (left), 8 (middle), and 12 (right) weeks following a single 50-Gy irradiation. B, Corresponding time course of T1-derived (top) and T2-derived (bottom) lesion volumes for both groups. One asterisk indicates $P < .05$; 3 asterisks, $P < .001$. *Abbreviation:* PIR = after irradiation.

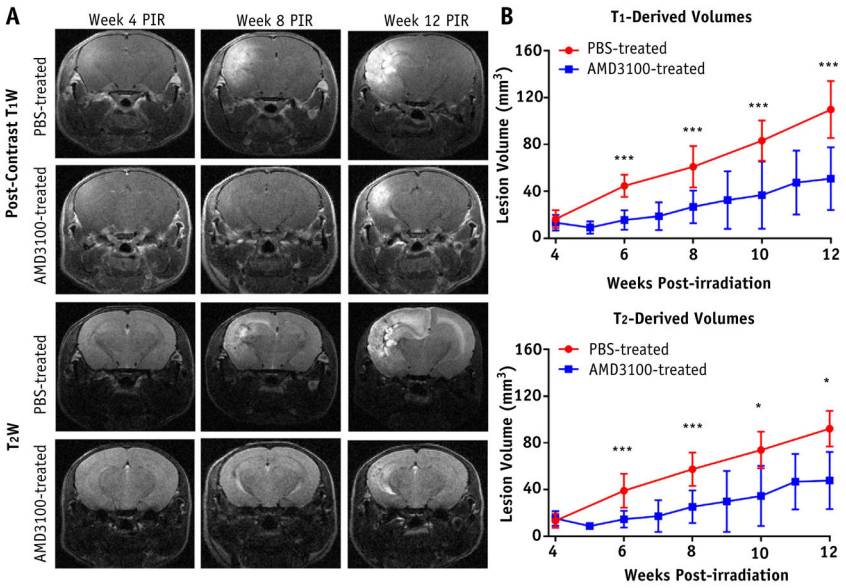

Fig. 2.

Treatment response with CXC chemokine receptor 4 (CXCR4) inhibitor, AMD3100, as detected by anatomic magnetic resonance imaging. A, Representative postcontrast T1-weighted (T1W) and T2-weighted (T2W) images acquired for phosphate-buffered saline solution (PBS)–treated (control) and AMD3100-treated groups at 3 time points after irradiation (PIR), similar to Fig. 1. B, Corresponding time course of lesion volumes for both groups. One asterisk indicates $P < .05$; 3 asterisks, $P < .001$.

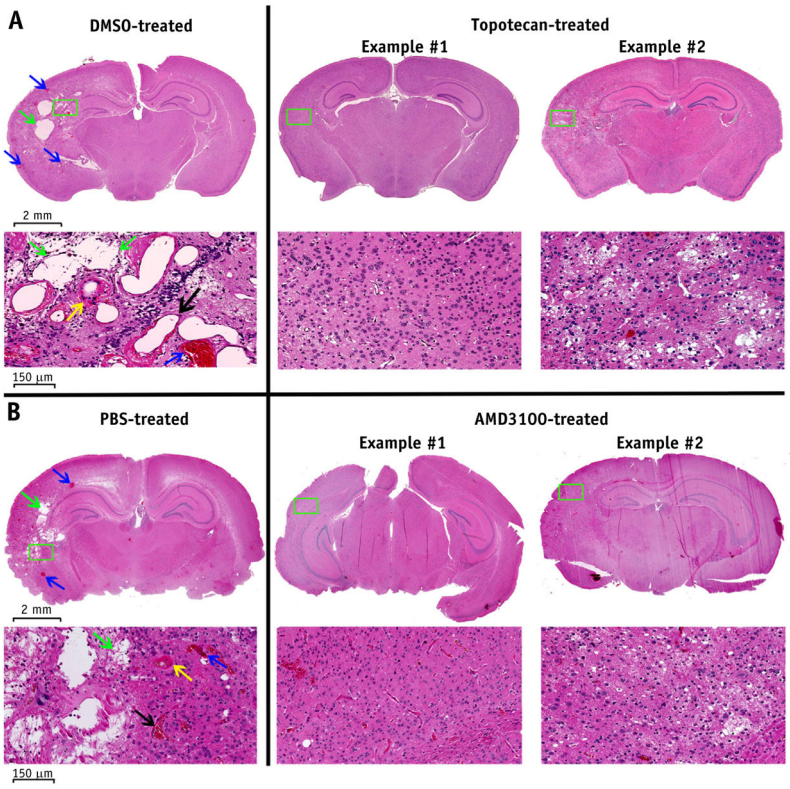

Fig. 3.

Hematoxylin-eosin staining demonstrates the treatment effects of both topotecan (A) and AMD3100 (B). Representative hematoxylin-eosin–stained histology slices with 1.25 × magnification (first and third rows) and 20 × magnification (second and fourth rows) are shown at week 12 after irradiation. The irradiated hemispheres of the control mice demonstrated histologic features that are characteristic of radiation necrosis, including fibrinoid vascular necrosis (yellow arrow), vascular telangiectasia (black arrow), hemorrhage (blue arrows), loss of neurons, and edema (green arrows), while these features were significantly reduced in severity in AMD3100-and topotecan-treated mice. *Abbreviations:* DMSO = dimethyl sulfoxide; PBS = phosphate-buffered saline solution.

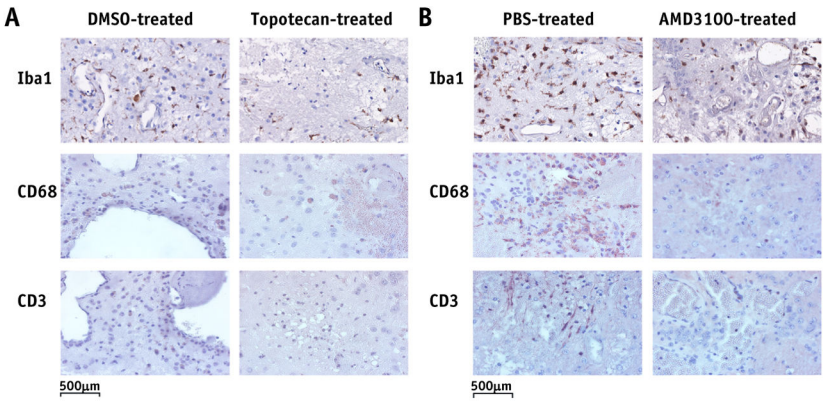

Fig. 4.

Immunohistochemistry-stained histology slices for Iba1, CD68, and CD3, which are markers for microglia, macrophages, and lymphocytes, respectively. Positive staining is indicated by a brown reaction product on a blue counterstain. Quantitative analysis of each of these stains across all animals is reported in Table 1 and discussed in the “Results” section.

Abbreviations: DMSO = dimethyl sulfoxide; Iba1 = ionized calcium-binding adapter molecule 1; PBS = phosphate-buffered saline solution.

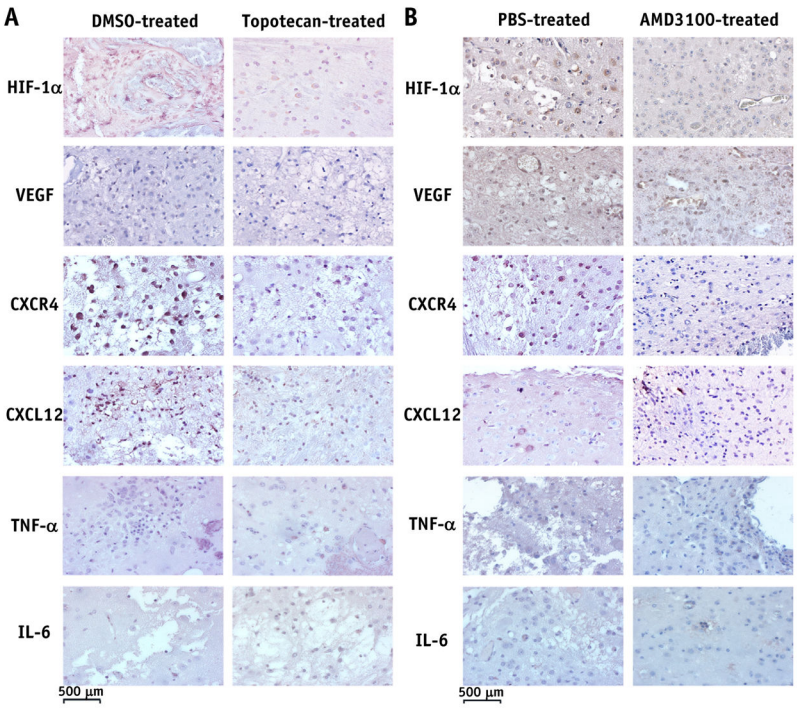

Fig. 5.

Immunohistochemistry-stained histology slices for hypoxia-inducible factor 1α (HIF-1α), vascular endothelial growth factor (VEGF), CXC chemokine receptor 4 (CXCR4), CXC chemokine ligand 12 (CXCL12), tumor necrosis factor α (TNF-α), and interleukin 6 (IL-6). Quantitative analysis of each of these stains across all animals is reported in Table 1 and discussed in the "Results" section. *Abbreviations:* DMSO = dimethyl sulfoxide; PBS = phosphate-buffered saline solution.

Table 1

Scoring of immunohistochemistry-stained slides

	AMD3100		Topotecan	
Stain	**Control**	**Treated**	**Control**	**Treated**
Iba1	2.8	2.3	3.0	2.2
CD3	1.3	0.0	1.8	0.3
CD68	2.8	0.5	2.8	0.3
TNF-α	3.0	1.5	2.6	0.8
IL-6	3.0	1.0	3.0	1.0
HIF-1α	2.3	1.8	2.7	2.3
VEGF	3.0	1.0	3.0	1.8
CXCR4	2.3	1.8	2.7	0.2
CXCL12	2.3	0.8	2.5	0.2

Abbreviations: CXCL12 = CXC chemokine ligand 12; CXCR4 = CXC chemokine receptor 4; HIF-1α = hypoxia-inducible factor 1α; Iba1 = ionized calcium-binding adapter molecule 1; IL-6 = interleukin 6; TNF-α = tumor necrosis factor α; VEGF = vascular endothelial growth factor.

Values represent the average score across all animals within each treatment or control group. Each immunohistochemistry stain was graded on a scale from 0 to 3 (ie, 0, no stain; 1, light stain; 2, moderate stain; and 3, heavy stain).